Creating and Transporting Trojan Wave Packets

B. Wyker,[1] S. Ye,[1] F. B. Dunning,[1] S. Yoshida,[2] C. O. Reinhold,[3,4] and J. Burgdörfer[2,4]

[1]*Department of Physics and Astronomy and the Rice Quantum Institute, Rice University, Houston, Texas 77005-1892, USA*
[2]*Institute for Theoretical Physics, Vienna University of Technology, Vienna, Austria, EU*
[3]*Physics Division, Oak Ridge National Laboratory, Oak Ridge, Tennessee 37831-6372, USA*
[4]*Department of Physics, University of Tennessee, Knoxville, Tennessee 37996, USA*
(Received 14 September 2011; published 24 January 2012)

Nondispersive localized Trojan wave packets with $n_i \sim 305$ moving in near-circular Bohr-like orbits are created and transported to localized near-circular Trojan states of higher n, $n_f \sim 600$, by driving with a linearly polarized sinusoidal electric field whose period is slowly increased. The protocol is remarkably efficient with over 80% of the initial atoms being transferred to the higher n states, a result confirmed by classical trajectory Monte Carlo simulations.

In quantum mechanics, all objects exhibit both particle-like and wavelike behaviors. One avenue for exploring this duality is analyzing the dynamics of wave packets, i.e., localized nonstationary wave functions, whose average motion mimics that of the corresponding classical particles. Indeed, Schrödinger suggested [1] that a localized coherent superposition of harmonic oscillator eigenstates [2] could be constructed that, due to the equispaced harmonic energy spectrum, would evolve without dispersion following the equations of motion for a classical particle. He also discussed the creation of coherent nondispersive electronic wave packets in atoms. However, in atoms, the energy levels are not equispaced, leading to dispersion and only transient localization [3,4]. Nonetheless, theory suggests that such dispersion can be suppressed with the aid of external fields [5–7]. The most intensively studied nondispersive states are termed Trojan wave packets [5,8] because the mechanism responsible for suppressing dispersion (of classical origin [9]) parallels that for formation of Jupiter's Trojan asteroids [8]. In the atomic physics analogue a localized Rydberg electron evolving along a circular ("planetary") orbit is stabilized by applying a circularly polarized microwave field synchronized with the orbital motion. Generation of such Trojan states has remained elusive. Recently, an attempt was made to create Trojan wave packets in Rydberg states ($n \sim 70$) from a low angular momentum ($\ell = 1$) state by adiabatically transforming a microwave driving field from elliptical to circular polarization [10]. However, the degree to which the ellipticity of the wave packet synchronously follows that of the microwave field remains an open question [11,12] as the circularly polarized field stabilizes not only circular wave packets but also non-Trojan low-ℓ states.

Here we pursue an alternative strategy for creating Trojan wave packets that utilizes linearly polarized fields [13]. The starting point is the generation of localized Rydberg wave packets moving in very-high-n (~ 305) near-circular orbits [4]. The Kepler periods for such states

are large, $T_n \simeq 4$ ns ($= 2\pi n^3$) (atomic units are used throughout), allowing their control using fast commercial pulse and arbitrary waveform generators. For example, unidirectional half-cycle pulses with duration $T_p \ll T_n$ can be produced. A scheme was recently demonstrated using a train of half-cycle pulses to maintain the localization of a near-circular wave packet over hundreds of orbits [14]. However, use of a unidirectional half-cycle pulse train, with its net dc field component, leads to a slow increase in the ellipticity of the orbit. Here we show that far superior stabilization can be achieved by driving with a linearly polarized sinusoidal field (which has no dc component) whose frequency is resonant with the wave packet and whose phase is synchronized with its orbital phase. This permits the simple and unambiguous realization of Trojan wave packets. Furthermore, we demonstrate that these Trojan wave packets are remarkably robust and can be adiabatically transported [15–17] to much higher $n \sim 600$, while preserving their circularity and localization, by chirping the frequency of the drive field. Creation of such states moves measurements a step closer to the macroscopic limit facilitating studies of classical-quantum correspondence [18].

The circular wave packets employed here are prepared, as described elsewhere [4], by first creating a mix of quasi-1D potassium Rydberg atoms with $n_i = 304$ and 306 oriented along the x axis by direct photoexcitation of selected redshifted Stark states in the presence of a weak ($\sim 400 \ \mu V \, cm^{-1}$) dc field [19]. This field is then turned off and a transverse electric pump field F_y^{pump} is suddenly applied along the $-y$ axis creating a wave packet that undergoes Stark precession [20,21]. After a time $T_{pump} = \pi/(3nF_y^{pump})$ this precession transforms the wave packet into a superposition of high-angular-momentum states ($\ell \sim m \sim n$) whereupon F_y^{pump} is turned off freezing the atom in a near-circular state in the xy plane. The subsequent evolution is monitored by the application, at $t = t_p$, of a probe field F_x^{probe} (or F_y^{probe}) along the x (or y) axis

sufficient to ionize a significant fraction of the atoms present. Depending on the choice of the probe field strength and duration, the resulting survival probability mirrors the time dependence of the expectation values of momentum, $\langle p_x(t_p) \rangle$ [or $\langle p_y(t_p) \rangle$], or of position, $\langle x(t_p) \rangle$ [or $\langle y(t_p) \rangle$] [22,23]. Additional information on the degree of circularity of the wave packet is given in the Supplemental Material [24]. The number of surviving atoms and their n distribution are measured by selective field ionization. Survival probabilities are determined by periodically monitoring the number of Rydberg atoms created through measurements with no pulsed fields applied.

Figure 1(a) shows survival probabilities measured as a function of the time delay between the turn-off of the pump field F_y^{pump} and application of a probe field F_y^{probe} to monitor $\langle y(t) \rangle$. The buildup of strong oscillations points to formation of a localized wave packet whose y coordinate varies sinusoidally as it orbits the nucleus. However, these oscillations damp at later times as localization is lost due to dephasing. (At much later times, $t \sim 450$ ns, the components of the wave packet move back into phase leading to strong quantum revivals [25].) As illustrated in Figs. 1(b) and 1(c), this dephasing can be suppressed by application,
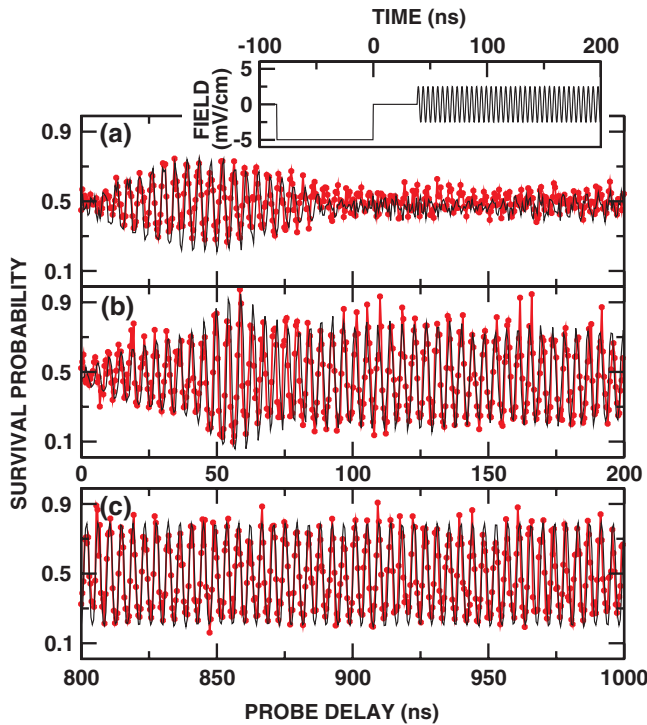
at the time of optimum localization, $t_L \sim 39$ ns, of a linearly polarized sinusoidal drive field $\vec{F}(t) \simeq \hat{y} F_{\text{drv}} \sin[\omega(t - t_L)]$ whose frequency, $\omega \sim \omega_{n_i} \sim n_i^{-3}$, matches the (average) Kepler frequency of the wave packet. The drive field is produced using a 2 gigasample/sec arbitrary waveform generator and is initiated when the wave packet is localized on the $+x$ axis moving in the $+y$ direction. Strong oscillations in survival probability are seen with little evidence of decay even after ~ 1 μs demonstrating the realization of a Trojan wave packet whose localization is maintained for many hundreds of orbits. A linearly polarized sinusoidal field corresponds to a superposition of two counterrotating circularly polarized fields, one of which corotates with the Trojan wave packet [13]. The counterrotating component averages to zero and can be neglected, the "rotating wave approximation." The suppression of dispersion, i.e., of broadening in the azimuthal angle $\phi = \arctan(y/x)$, by the corotating circularly polarized component, results from the torque it exerts. Trajectories slightly advanced (delayed) in ϕ compared to the rotating field $\vec{F}$ suffer a torque
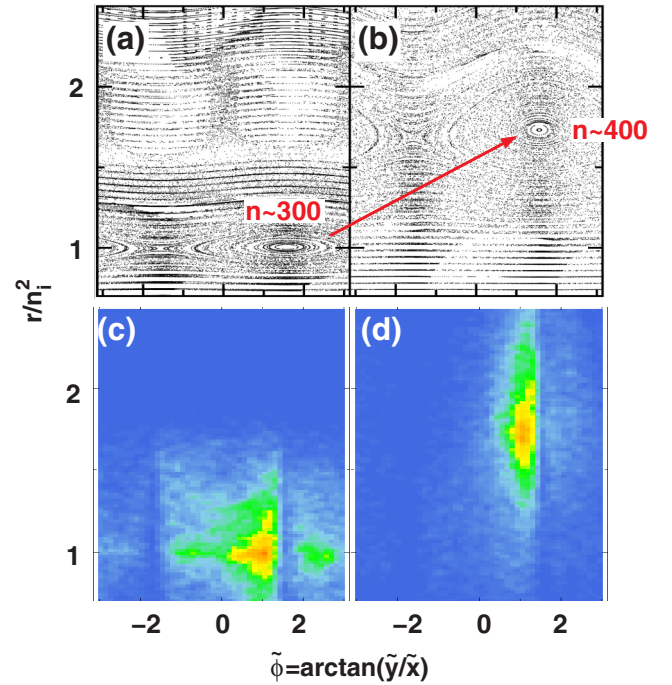

FIG. 1 (color online). Experimental (symbols) and calculated (lines) survival probabilities versus the time of application of a 6 ns, 100 mV cm^{-1} probe pulse after turn-off of an 85 ns, 5 mV cm^{-1} pump pulse. (a) Results with no drive field present, (b),(c) results with 2.5 mV cm^{-1}, 230 MHz sinusoidal drive field initiated at $t_L \sim 39$ ns. The pump, drive, and probe fields are all applied along the y axis. The inset shows the pulse sequence applied to the parent quasi-1D atoms.

FIG. 2 (color online). Poincaré surfaces of section for a Rydberg atom driven by a linearly polarized field $\vec{F}(t) \simeq \hat{y} F_{\text{drv}} \sin[\omega(t - t_L)]$ with $F_{\text{drv}} = 2.5$ mV cm^{-1} and values of ω of (a) 230 MHz and (b) 104 MHz. The surfaces of section $(r/n_i^2, \tilde{\phi})$ in the rotated frame are obtained by cutting phase space at $L \simeq n$ and $L_y \simeq 0$. The stroboscopic snapshots are taken when $\vec{F}(t)$ reaches its maximum, i.e., at $\omega(t - t_L) = \pi/2$ (modulo 2π). (c),(d) Initial and final spatial densities in the $(r/n_i^2, \tilde{\phi})$ plane for a near-circular $n_i = 305$ wave packet driven by a sinusoidal field with $F_{\text{drv}} = 2.5$ mV cm^{-1} chirped from 230 to 104 MHz over 1 μs.

$$\frac{dL_z}{dt} = \hat{z} \cdot (\vec{r} \times \vec{F}) \propto -rF_{\mathrm{drv}} \sin\Delta\phi, \qquad (1)$$

where $\Delta\phi$ is the angle between the electron coordinate $\vec{r}$ and $\vec{F}$. For trajectories with $\Delta\phi > 0$ ($\Delta\phi < 0$) the angular motion is decelerated (accelerated) leading to stabilization near $\Delta\phi = 0$, i.e., $\phi = \omega t$. Classical Poincaré surfaces of section [stroboscopic snapshots of the phase space (see Fig. 2)] reveal the existence of stable islands around $\phi = \omega t$ [9]. Because of the cylindrical symmetry of the drive field with respect to the y axis, the system is effectively two dimensional and, for $L \simeq 0$, each trajectory is confined to a plane sharing the y axis. We therefore introduce a new coordinate system $(\tilde{x}, \tilde{y})$ by rotating the plane of orbit for each trajectory so that they are all confined to the $\tilde{x}\tilde{y}$ plane. The surfaces of section are taken in the $(r, \tilde{\phi})$ plane [$\tilde{\phi} = \arctan(\tilde{y}/\tilde{x})$] by cutting the phase space at $|L| \simeq n$ and $L_y \simeq 0$. The stable islands are centered at $\tilde{\phi} = \pi/2$ and $r = n^2$ (or $|\omega|^{-2/3}$). The drive frequencies in Figs. 2(a) and 2(b) correspond to $n = n_i \sim 305$ and $n \sim 400$, respectively. Since the units are scaled to $n_i = 305$, the stable island in Fig. 2(b) appears at $r_0 = r/n_i^2 = 1.7$.

Because of the close quantum-classical correspondence in high Rydberg manifolds, the stabilization present in the quantum-mechanical atom can be described using classical trajectory Monte Carlo simulations [26] where an ensemble of points in phase space is used to represent the wave packet. Initially, the ensemble approximates the phase space density of the initial mix of Stark states [19]. Its time evolution is followed by solving the Hamilton equation of motion for each trajectory leading to predictions that agree well with the measured results (see Fig. 1). Localization of a wave packet within the stable island suggests that if its position is changed near-adiabatically by, say, slowly down-chirping the frequency of the drive field, the wave packet might remain trapped and be transported to near-circular states of substantially higher n [16]. The chirp rate, $|(\omega_f - \omega_i)/T_{\mathrm{chirp}}|$, where $\omega_{f,i} = n_{f,i}^{-3}$ and T_{chirp} the transition time from ω_i to ω_f, must be sufficiently slow that the atom can respond adiabatically. For small changes in n, transport can be accomplished using a chirped field of constant amplitude,

$$F(t + t_L) = F_{\mathrm{drv}} \sin\left(\omega_i t + \frac{\omega_f - \omega_i}{2T_{\mathrm{chirp}}} t^2\right). \qquad (2)$$

However, as the atom moves towards states of much higher n, the amplitude of the drive field must be reduced to preserve the size of the stable island and to limit field-induced ionization. A drive field of the form

$$F(t + t_L) = \frac{F_{\mathrm{drv}} n_i^4}{n(t)^4} \sin\left(\omega_i t + \frac{\omega_f - \omega_i}{2T_{\mathrm{chirp}}} t^2\right) \qquad (3)$$
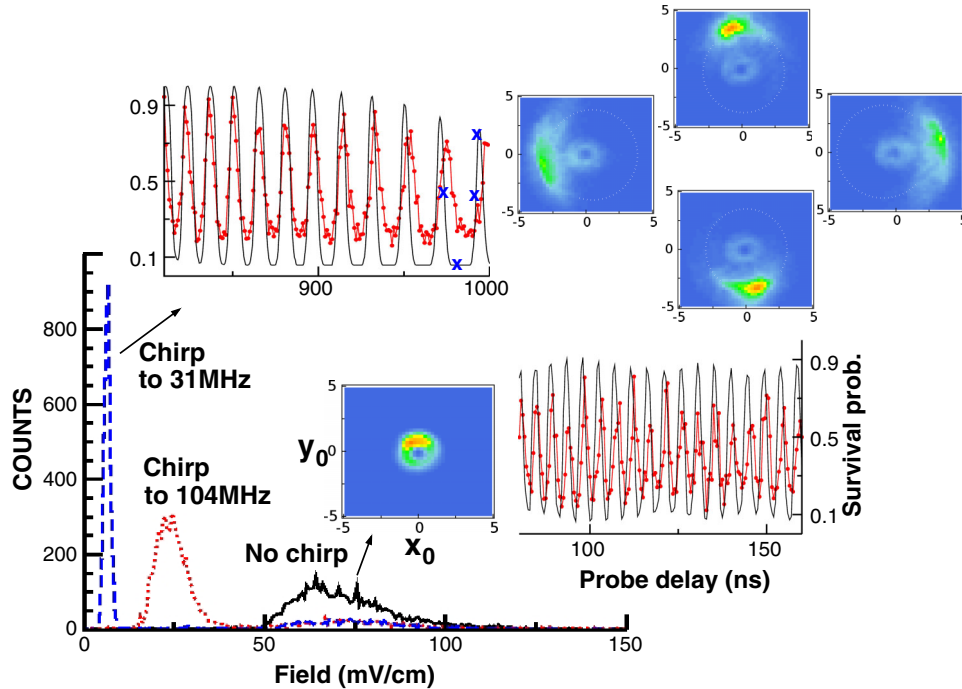

FIG. 3 (color online).   Selective field ionization spectra showing ionization signals observed as a function of field applied along the y axis. The spectra were obtained after driving by (black line) an unchirped sinusoidal drive field as in Fig. 1, (red dotted line) the same chirped drive field as for Fig. 2(d), and (blue dashed line) the same drive field as for Fig. 4. The graphical insets show measured (symbols) and calculated (line) survival probabilities versus time of application of a 6-ns-long probe pulse sufficient to ionize, on average, $\sim 50\%$ of the atoms. The other insets show snapshots of the calculated spatial distributions in the $x_0 y_0$ plane ($x_0, y_0 = x, y/n_i^2$) for the conditions or times indicated (crosses).

with $\omega_i + (\omega_f - \omega_i)t/T_{\text{chirp}} = 1/n(t)^3$ will preserve the scaled field strength at all times during transport. In practice, a simple linear variation in amplitude also works well.

Figures 2(c) and 2(d) show simulations of the initial and final spatial distributions for $n_i \sim 305$ atoms subject to a linearly chirped drive field, Eq. (2), with $\omega_i \sim 230$ MHz, $\omega_f \sim 104$ MHz, $T_{\text{chirp}} \sim 1$ μs, and $F_{\text{drv}} = 2.5$ mV cm^{-1}, equivalent to driving from $n_i \sim 305$ to $n_f \sim 400$. The great majority ($> 80\%$) of the electron trajectories lock to the drive field and are transported to $n_f \sim 400$, i.e., from states localized at $r_i \sim n_i^2$ to $r_f \sim n_f^2 \sim 1.7 n_i^2$. Remarkably, the transfer can be extended to much higher n if the amplitude of the drive field is reduced. This is illustrated in Fig. 3 for a frequency chirp from $\omega_i \sim 230$ MHz to $\omega_f \sim 31$ MHz, again over $T_{\text{chirp}} \sim 1$ μs. The energy distribution remains narrow and moves steadily towards states of higher n ending near $n_f \sim 600$ ($\omega_{n_f} \sim 31$ MHz). (A small fraction of the trajectories do not lock to the field and suffer little change in n.) Transport to higher n leads to an increase in the amplitude and to a decrease in the frequency of the oscillations in $\langle x(t) \rangle$ and $\langle y(t) \rangle$ [Fig. 4(a)] and a decrease in the amplitude of the oscillations in $\langle p_x(t) \rangle$ and $\langle p_y(t) \rangle$ [Fig. 4(b)]. The final amplitude of $\langle x(t) \rangle$ is smaller than $\langle y(t) \rangle$. It is important to note that this does not necessarily indicate increased ellipticity in the present case. Quite the contrary, the distribution of scaled angular momenta perpendicular to the $\tilde{x}\tilde{y}$ orbital plane $L_{\perp 0} = \tilde{L}_z/n = \sqrt{L_x^2 + L_z^2}/n$ becomes narrower [see Fig. 4(d)] and peaks at $L_{\perp 0} = 1$, indicating that the final state is actually more circular than the initial state. The distribution of orbital planes results because the initial wave packet generated from the quasi-1D state includes near-circular trajectories whose angular momenta are large in magnitude but whose directions are not perfectly aligned with the z axis. These "misaligned" wave packets are equally stable and their motions display larger oscillations in $\langle y(t) \rangle$ than in $\langle x(t) \rangle$.

The simulations in Figs. 2(d) and 4 are confirmed experimentally by the selective field ionization (SFI) spectra in Fig. 3 recorded under identical driving conditions. With no chirping, a single SFI feature is seen that matches well that seen immediately after turn-off of the pump field indicating that application of a (resonant) drive field leads to very little energy broadening. With chirping, the SFI spectrum changes markedly and moves to lower fields indicative of the population of higher n states. The widths and positions of the peaks are similar to those seen following direct excitation of (low-ℓ) states with $n \sim 400$ and $n \sim 600$ showing that chirping indeed populates a narrow distribution of higher-n states. A small later-time feature remains in both spectra that corresponds to ionization of states with $n \sim n_i$ demonstrating that, as suggested by the simulations, a small part ($< 20\%$) of the parent wave
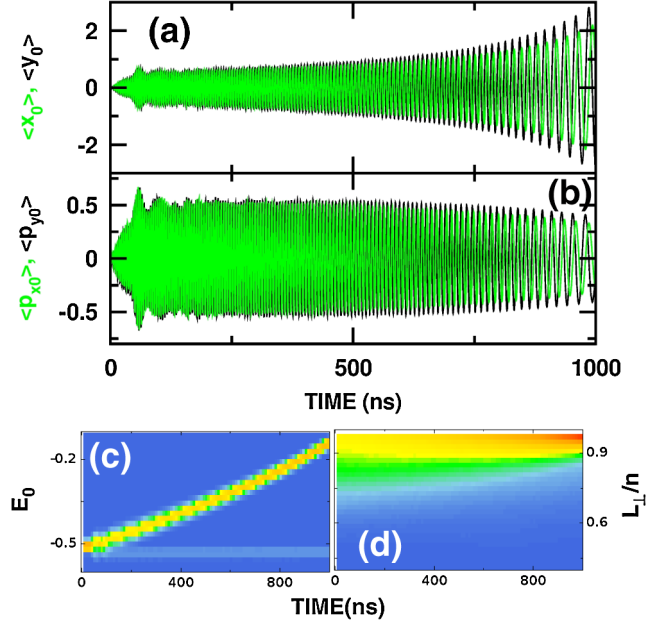

FIG. 4 (color online). Evolution of (a) $\langle x(t) \rangle$, $\langle y(t) \rangle$, (b) $\langle p_x(t) \rangle$, $\langle p_y(t) \rangle$, (c) the energy distribution, and (d) the distribution of scaled transverse angular momentum for a near-circular $n_i \sim 305$ wave packet initially localized in the xy plane and subject to a sinusoidal drive field whose frequency is chirped from 230 to 31 MHz over 1 μs, while linearly decreasing its amplitude from 2.5 to 1.3 mV cm^{-1}. The spatial coordinates, momenta, and energy are scaled to n_i: $x_0, y_0 = x, y/n_i^2$, $p_{x0}, p_{y0} = n_i p_x, n_i p_y$, and $E_0 = n_i^2 E$. The angular momentum $L_\perp$ is scaled to the time dependent n.

packet is not positioned within the stable island and is not transported to higher n states.

The production of very-high-n wave packets is further demonstrated by the changing periods of the oscillations in survival probability observed during chirping (see insets in Fig. 3), the period changing from the Kepler period for $n_i \sim 305$ to that for $n \sim 600$. The large amplitude of the oscillations, which are in good agreement with simulations, demonstrate that the wave packet remains circular and locked to the drive field. (Similar oscillations are seen with the probe field applied along the x axis also consistent with the creation of a high-ℓ wave packet.) Remarkably, simulations suggest that transport to $n \simeq 600$ results in even better localization (see insets in Fig. 3).

The present work presents an unambiguous realization of nondispersive Trojan wave packets in very high n atoms using sinusoidal driving fields. Their remarkable stability might be exploited to trap coherent circular states and prevent their dephasing (almost) indefinitely. The ability to generate very-high-n near-circular Bohr-like states provides a necessary first step towards creating long-lived two-electron excited states [27]. The first excited electron remains well separated from the core ion which then behaves as an isolated particle. For alkaline earth metals such as strontium, the core ion is optically accessible

facilitating excitation of a second inner electron [28]. Because the outer very-high-n electron is only weakly coupled to the core ion, the resulting two-electron excited states will not undergo rapid autoionization, rather the core ion will fluoresce allowing the Rydberg atom to be imaged and to be optically trapped. Excitation of an inner electron to a high-n state also admits the possibility of creating "planetary atoms" [29–31] in stable highly correlated multiply excited states.

[1] E. Schrödinger, Naturwissenschaften **14**, 664 (1926).

[2] R. J. Glauber, Phys. Rev. Lett. **10**, 84 (1963).

[3] L. S. Brown, Am. J. Phys. **41**, 525 (1973).

[4] J. J. Mestayer et al., Phys. Rev. Lett. **100**, 243004 (2008).

[5] M. Kalinski and J. H. Eberly, Phys. Rev. A **53**, 1715 (1996).

[6] A. F. Brunello, T. Uzer, and D. Farrelly, Phys. Rev. Lett. **76**, 2874 (1996).

[7] A. Buchleitner, D. Delande, and J. Zakrzewski, Phys. Rep. **368**, 409 (2002).

[8] I. Bialynicki-Birula, M. Kaliński, and J. H. Eberly, Phys. Rev. Lett. **73**, 1777 (1994).

[9] D. Farrelly and T. Uzer, Phys. Rev. Lett. **74**, 1720 (1995).

[10] H. Maeda, J. H. Gurian, and T. F. Gallagher, Phys. Rev. Lett. **102**, 103001 (2009).

[11] S. Yoshida, C. O. Reinhold, J. Burgdörfer, and F. B. Dunning, Phys. Rev. Lett. **103**, 149301 (2009).

[12] H. Maeda, J. H. Gurian, and T. F. Gallagher, Phys. Rev. Lett. **103**, 149302 (2009).

[13] M. Kalinski and J. H. Eberly, Phys. Rev. A **52**, 4285 (1995).

[14] J. J. Mestayer et al., Phys. Rev. A **79**, 033417 (2009).

[15] B. Meerson and L. Friedland, Phys. Rev. A **41**, 5233 (1990).

[16] M. Kalinski and J. H. Eberly, Opt. Express **1**, 216 (1997).

[17] H. Maeda, D. V. L. Norum, and T. F. Gallagher, Science **307**, 1757 (2005).

[18] C. R. Stroud, Jr., Physics **2**, 19 (2009).

[19] C. L. Stokely et al., Phys. Rev. A **67**, 013403 (2003).

[20] D. Richards, J. Phys. B **17**, 1221 (1984).

[21] D. Delande and J. C. Gay, Europhys. Lett. **5**, 303 (1988).

[22] M. B. Campbell, T. J. Bensky, and R. R. Jones, Phys. Rev. A **58**, 514 (1998).

[23] B. E. Tannian, C. L. Stokely, F. B. Dunning, C. O. Reinhold, and J. Burgdörfer, Phys. Rev. A **64**, 021404 (2001).

[24] See Supplemental Material at http://link.aps.org/supplemental/10.1103/PhysRevLett.108.043001 for more details.

[25] C. O. Reinhold et al., J. Phys. B **42**, 091003 (2009).

[26] R. Abrines and I. C. Percival, Proc. Phys. Soc. London **88**, 861 (1966).

[27] M. Kalinski, J. H. Eberly, J. A. West, and C. R. Stroud, Jr., Phys. Rev. A **67**, 032503 (2003).

[28] U. Eichmann, V. Lange, and W. Sandner, Phys. Rev. Lett. **64**, 274 (1990).

[29] I. C. Percival, Proc. R. Soc. A **353**, 289 (1977).

[30] S. N. Pisharody and R. R. Jones, Science **303**, 813 (2004).

[31] T. Uzer, D. Farrelly, J. A. Milligan, P. E. Raines, and J. P. Skelton, Science **253**, 42 (1991).